Afghanistan Journal of Infectious Diseases
AJID
https://ajid.ghalib.edu.af/index.php/ajid

January 2026, Vol. 4, No.1, pp:94-113

Comparative Analysis of Runge–Kutta and Backward Euler Methods for Modeling Monkeypox Transmission Dynamics

*Zabihullah Movaheedi [1], Abdul Razeq Rahmani [2]

1. *Department of Mathematics, Faculty of Science, Herat University, Herat, Afghanistan*
2. *Mathematics Department, Education Faculty, Farah University, Farah, Afghanistan*

ARTICLE INFO

Type: Original Article
Received: 17/10/2025
Accepted: 30/12/2025

*Corresponding Author:
E-mail address:
z.movaheedi2@gmail.com

To cite this article:

Movaheedi Z, Rahmani AR. Comparative Analysis of Runge–Kutta and Backward Euler Methods for Modeling Monkeypox Transmission Dynamics. Afghan J Infect Dis. 2026; 4(1): pp:94-113.

DOI:
https://doi.org/10.60141/ajid.142

ABSTRACT

Background: Monkeypox (Mpox) is a re-emerging zoonotic viral disease that poses an increasing threat to global public health. Mathematical modeling is a key tool for understanding transmission dynamics of diseases like Mpox and supporting effective control strategies. Reliable numerical methods are essential for solving the nonlinear differential equations arising from such models.
Materials: We developed a deterministic compartmental model to describe Mpox transmission between human and small mammal populations. Human compartments include susceptible, exposed, infected, isolated, and recovered individuals, with corresponding classes for small mammals. We solved the system of nonlinear ordinary differential equations using the fourth-order Runge–Kutta (RK4) method and the Backward Euler method. We validated the model using real outbreak data from the U.S. Clade II Mpox cases reported by the Centers for Disease Control and Prevention (CDC, 2025).
Results: Simulation results demonstrate that RK4 provides higher accuracy and faster convergence in non-stiff scenarios, making it suitable for short-term epidemic predictions. The Backward Euler method exhibits superior numerical stability for stiff systems, allowing reliable long-term simulations with larger time steps. Error and computational analyses confirm RK4's efficiency, while Backward Euler ensures robustness in unstable dynamic regions. Data fitting verifies that RK4 produces closer short-term approximations, whereas Backward Euler yields smoother long-term trends.
Conclusion: Both numerical methods are effective for modeling Mpox transmission. RK4 is recommended for accurate short-term analysis, while Backward Euler is preferable for stiff epidemic dynamics requiring high stability. These results highlight the importance of appropriate numerical method selection in computational epidemiology.

Keywords: Backward Euler Method, Compartmental Model, Mpox Transmission, Numerical Methods, Runge-Kutta Method

Introduction

Monkeypox (Mpox) has re-emerged in recent years as a significant global public health threat, marked by recurrent outbreaks across multiple continents. As a zoonotic orthopoxvirus with transmission routes involving both human–human and animal–human interactions, Mpox exhibits complex epidemiological characteristics that necessitate rigorous mathematical investigation. Understanding its transmission dynamics is crucial not only for predicting epidemic trajectories but also for designing timely and effective intervention strategies such as vaccination, isolation, and mobility restrictions (1–3). Compartmental models—including SIR, SEIR, and their extended structures—remain indispensable analytical tools in such studies and have been successfully applied to Mpox and related infectious diseases (4–7).

The growing diversity of modeling approaches in the recent literature highlights the need for flexible mathematical frameworks that can capture key biological, environmental, and behavioral features of emerging pathogens. For instance, fractional-order models have been utilized to examine Mpox transmission under vaccination interventions (8), while delay differential equation frameworks have been applied to assess vaccination-driven cholera dynamics (9). Similarly, fractional epidemic models have provided new insights into the transmission behavior of the Marburg virus, demonstrating the broader usefulness of non-standard dynamical tools for studying emerging zoonoses (10). These studies collectively emphasize that accurate modelling depends not only on well-structured epidemiological assumptions but also on the efficient and reliable numerical solution of the underlying system of nonlinear differential equations.

Because analytical solutions to such systems are rarely available, numerical methods play a foundational role in computational epidemiology. The selection of an appropriate solver directly influences the accuracy, stability, and computational cost of simulations. Explicit methods such as the classical 4th-order Runge–Kutta (RK4) scheme are widely used for their simplicity, high accuracy, and effectiveness in non-stiff epidemic systems (6,11). However, epidemic models often exhibit stiff behavior—particularly during rapid changes in incidence, strong isolation effects, or high-frequency transmission events—where explicit schemes may fail or require prohibitively small step sizes. In such settings, implicit solvers like the Backward Euler method offer superior stability and robustness, making them more suitable for long-term projections and stiff epidemic phases (12, 13).

Despite the extensive use of these numerical schemes in epidemiological modeling, direct comparative analyses that evaluate their performance on Mpox transmission models remain limited. Therefore, there is a clear need to systematically assess how explicit and implicit numerical solvers behave when applied to complex epidemic systems with interacting human and animal hosts.

Motivated by this gap, the present study provides a detailed comparative analysis of the RK4 and Backward Euler methods in the context of a two-population Mpox transmission mode. By examining accuracy, stability properties, convergence behavior, and computational efficiency, we aimed to identify the most suitable numerical approach for different epidemic scenarios. Such an analysis not only improves methodological understanding but also aims to support the development of more reliable computational frameworks for future Mpox forecasts and broader infectious disease modeling applications, thereby enhancing the robustness and credibility of numerical epidemic simulations.

Methods

Mathematical Modeling of Mpox Transmission

We introduce a deterministic compartmental model to illustrate the transmission dynamics of Mpox, focusing on two primary populations: humans and small mammals. The human population is divided into five compartments: susceptible individuals $S_i(t)$, exposed individuals $E_i(t)$, infected individuals $I_i(t)$, isolated individuals $Q_i(t)$, and recovered individuals $R_i(t)$. The small mammal population consists of three compartments: susceptible small mammals $S_s(t)$, exposed small mammals $E_s(t)$, and infected small mammals $I_s(t)$. Individuals enter the human population at a recruitment rate of θ_i, while small mammals are recruited at a rate of θ_s. Transmission from infected small mammals to humans occurs at a force of infection represented by β_1, and human-to-human transmission occurs at rate β_2. Likewise, transmission among small mammals is governed by β_3, which denotes the force of infection from infected small mammals to susceptible ones. Exposed humans progress to the infected class at rate α_1, and some exposed individuals transition to the isolated class at rate α_2. Exposed small mammals transition to the infected small mammal class at rate α_3. A fraction of isolated humans who are not infected return to the susceptible class at rate ϕ. Confirmed isolated cases further progress to the infected class at rate τ, and infected humans recover at rate Δ. Natural mortality affects humans and small mammals at rates μ_i and μ_s, respectively. Disease-induced death occurs at rate δ_i for infected humans and δ_s for infected small mammals. The transitions between these compartments are illustrated in Figure 1.

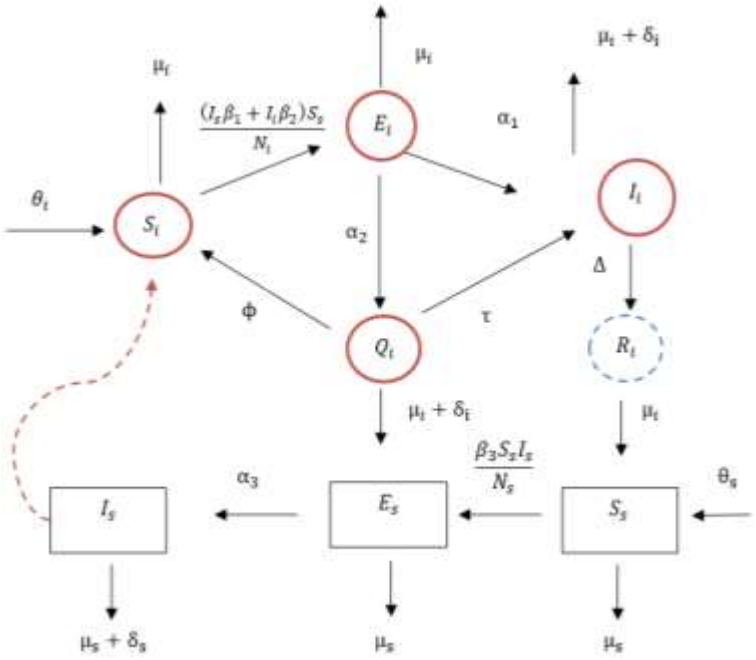

Figure 1: Schematic overview of the model structure

The following set of nonlinear differential equations describes the model's dynamics. Table 1 provides the values, sources, and descriptions of all parameters used in (Eq. 1).

$$\frac{dS_i}{dt} = \theta_i - (\beta_1 I_s + \beta_2 I_i)\frac{S_i}{N_i} - \mu_i S_i + \phi Q_i$$
$$\frac{dE_i}{dt} = (\beta_1 I_s + \beta_2 I_i)\frac{S_i}{N_i} - (\alpha_1 + \alpha_2 + \mu_i)E_i$$
$$\frac{dI_i}{dt} = \alpha_1 E_i - (\mu_i + \delta_i + \Delta)I_i$$
$$\frac{dQ_i}{dt} = \alpha_2 E_i - (\phi + \tau + \delta_i + \mu_i)Q_i \qquad \text{(Eq. 1)}$$
$$\frac{dR_i}{dt} = \tau Q_i + \Delta I_i - \mu_i R_i$$
$$\frac{dS_s}{dt} = \theta_s - \beta_3 S_s I_s \frac{1}{N_s} - \mu_s S_s$$
$$\frac{dE_s}{dt} = \beta_3 S_s I_s \frac{1}{N_s} - (\mu_s + \alpha_3)E_s$$
$$\frac{dI_s}{dt} = \alpha_3 E_s - (\mu_s + \delta_s)I_s.$$

Table 1: Parameters values used in the Simulations.

Parameter	***Description***	***Value***	***Unit***	***Reference***
θ_i	Rate of recruitment into the human population	1,160,000	Year $^{-1}$	Estimated
θ_s	Recruitment rate for the small mammal population	200000	Year $^{-1}$	Estimated
β_1	Force of infection from Small mammals to Human	0.0025	Year $^{-1}$	(14)
β_2	Force of infection from Human to Human	0.000063	Year $^{-1}$	(14)
β_3	Force of infection from Small mammals to Small mammals	0.0027	Year $^{-1}$	(14)
α_1	Rate of transition from exposed human to infected human	0.2	Year $^{-1}$	(15)
α_2	Transition rate from exposed to isolated cases	2.0	Year $^{-1}$	(15)
α_3	Transition from exposed small mammals to infected small mammals	3.0	Year $^{-1}$	Assumed
φ	Fraction of those isolated that is not infected	2.0	Year $^{-1}$	(15)
τ	Progression from isolated to infected class	0.52	Year $^{-1}$	(15)
Δ	Humans recovery rate	0.83	Year $^{-1}$	(16)
μ_i	Natural death rate of human	0.008	Year $^{-1}$	(17)
μ_s	Natural death rate of small mammals	0.002	Year $^{-1}$	(14)
δ_s	Disease induced death rate for small mammals	0.5	Year $^{-1}$	(15)
δ_i	Death rate due to disease for humans	0.2	Year $^{-1}$	(18)

The model analysis

On Human Population, $N_i = S_i + E_i + I_i + Q_i + R_i$, the differential equation is given as: $\frac{dN_i}{dt} = \theta_i - \delta_i I_i - \mu_i N_i$.

Also, for the small mammal population $N_s = S_s + E_s + I_s$, and the associated differential equations are as follows:

$\frac{(dN_s)}{dt} = \theta_s - (\mu_s + \theta_s)N_s$.

Theorem 1: *Let* $(S_i, E_i, I_i, Q_i, R_i, S_s, E_s, \mathbb{R})$ represent the solution of (Eq.1), given initial conditions within a biologically feasible region $\Delta = \Delta_i \times \Delta_s$ *with:*

$$\Delta_i = (S_i, E_i, I_i, Q_i, R_i) \in \mathbb{R}^5_+ : N_i \leq \frac{\theta_i}{\mu_i}$$

and

$$\Delta_s = (S_s, E_s, R_r) \in \mathbb{R}^3_+ : N_s \leq \frac{\theta_s}{\mu_s},$$

then Δ is a non-negative invariant set.

Following the method of Rana and Sharma (19), it follows that:

$$0 \leq N_i(t) \leq N_i(0) l^{-\mu_i(t)} + \frac{\theta_i}{\mu_s}\left(1 - l^{-\mu_i(t)}\right)$$

also

$$N_s(t) \leq N_s(0) l^{-(\mu_s+\theta)t} + \frac{\theta_s}{\mu_s}\left(1 - l^{-(\mu_s+\theta)t}\right),$$

hence for t, the set Δ is positive invariant.

Mpox-Free Equilibrium State

This state occurs when no disease is present. Therefore, in the absence of infection, we set E_i, I_i, Q_i, R_i, E_s and I_s to zero in (Eq. 1), and the resulting solution yields the Mpox-free equilibrium states expressed as:

$$\Phi_{MFE}(S_i{}^*, E_i{}^*, I_I{}^*, Q_i{}^*, R_i{}^*, S_s{}^* E_s{}^*, I_s{}^*)$$

.

Endemic equilibrium

This occurs when the infection remains present in the population, represented b

y $\Phi_{MEE}(S_i^*, E_i^*, I_i^*, Q_i^*, R_i^*, S_s^*, E_i^*, I_s^*)$. Thus,

$$\begin{aligned} S_i^* &= \frac{k_1 k_3 \theta_i}{\mu_i k_1 k_3 - \alpha_2 \varphi \phi_i + k_1 k_3 \phi_i}, E^*{}_i \\ &= \frac{k_3 \phi_i \theta_i}{\mu_i k_1 k_3 - \alpha_2 \varphi \phi_i + k_1 k_3 \phi_i}, I^*{}_i \\ &= \frac{k_3 \alpha_1 \phi_i \theta_i}{k_2(\mu_i k_1 k_3 - \alpha_2 \varphi \phi_i + k_1 k_3 \phi_i)}, Q^*{}_i \\ &= \frac{\alpha_2 \phi_i \theta_i}{\mu_i k_1 k_3 - \alpha_2 \varphi \phi_i + k_1 k_3 \phi_i}, R^*{}_i \\ &= \frac{(\alpha_1 \gamma k_3 + \alpha_2 k_2 \tau)\phi_i \theta_i}{\mu_i k_2(\mu_i k_1 k_3 - \alpha_2 \varphi \phi_i + k_1 k_3 \phi_i)}, Q^*{}_s \\ &= \frac{\theta_s}{\mu_s + \phi_s}, E^*{}_s = \frac{\theta_s}{k_4(\mu_s + \phi_s)}, I_s^* \\ &= \frac{\phi_s \alpha_3 \theta_s}{k_4 k_5(\mu_s + \phi_s)}. \end{aligned}$$

Where,

$k_1 = \alpha_1 + \alpha_2 + \mu_i$, $k_2 = \mu_i + \delta_i +$, $k_3 = \varphi + \tau + \delta_i + \mu_i, k_4 = \mu_s + \alpha_3$, $k_5 = \mu_s + \delta_s$,

$\phi_i = \frac{\beta_1 I_s^* + \beta_2 I_i^*}{N_i}, \phi_s = \frac{\beta_3 I^*}{N_s}$.

Basic reproduction number

Let the infected state variables be ordered as

$$x = (E_i, I_i, Q_i, E_s, I_s)^{\mathrm{T}}.$$

The Mpox-free equilibrium (MFE) of system (Eq. 1) is

$$\begin{aligned} \Phi_{\mathrm{MFE}} &= (S_i^*, E_i^*, I_i^*, Q_i^*, R_i^*, S_s^*, E_s^*, I_s^*) \\ &= \left(\frac{\theta_i}{\mu_i}, 0,0,0,0, \frac{\theta_s}{\mu_s}, 0,0\right). \end{aligned}$$

Following the next-generation matrix (NGM) approach of van den Driessche and Watmough (17), we decompose the infected subsystem in the form

$$\frac{dx}{dt} = F(x) - V(x),$$

where $F_i(x)$ denotes the rate of appearance of new infections in compartment i, and $V_i(x)$ collects all other transitions (progression, recovery, isolation, natural and disease-induced mortality). The Jacobian matrices of F and V evaluated at the MFE are denoted by F and V, and the basic reproduction number is

$$R_0 = \rho(FV^{-1}),$$

the spectral radius of the next-generation matrix. New infection matrix F. New infections occur only in the exposed human class E_i (from I_i and I_s) and in the exposed small-mammal class E_s (from I_s). Linearising at the MFE (so that $\frac{S_i^*}{N_i} =$ 1 and $\frac{S_s^*}{N_s} = 1$) yields

$$F = \begin{pmatrix} 0 & \beta_2 & 0 & 0 & \beta_1 \\ 0 & 0 & 0 & 0 & 0 \\ 0 & 0 & 0 & 0 & 0 \\ 0 & 0 & 0 & 0 & \beta_3 \\ 0 & 0 & 0 & 0 & 0 \end{pmatrix}.$$

Transition matrix V. Let

$$\begin{aligned} k_1 &= \alpha_1 + \alpha_2 + \mu_i, \\ k_2 &= \mu_i + \delta_i + \gamma, \\ k_3 &= \phi + \tau + \delta_i + \mu_i, \\ k_4 &= \mu_s + \alpha_3, \\ k_5 &= \mu_s + \delta_s. \end{aligned}$$

Then the Jacobian of the non-infection transitions is

$$V = \begin{pmatrix} k_1 & 0 & 0 & 0 & 0 \\ -\alpha_1 & k_2 & 0 & 0 & 0 \\ -\alpha_2 & 0 & k_3 & 0 & 0 \\ 0 & 0 & 0 & k_4 & 0 \\ 0 & 0 & 0 & -\alpha_3 & k_5 \end{pmatrix}.$$

Because V is block-lower-triangular, its inverse is obtained blockwise. Only the columns corresponding to infectious classes I_i and I_s are needed:

$$V^{-1}e_2 = \left(0, \frac{1}{k_2}, 0,0,0\right)^{\mathrm{T}}, V^{-1}e_5 = \left(\frac{0,0,0,0,1}{k_5}\right)^{\mathrm{T}},$$

here e_2 and e_5 is the unit vectors in $\mathbb{R}^5$. Next-generation matrix. Multiplying gives

$$K = FV^{-1} = \begin{pmatrix} 0 & \frac{\beta_2}{k_2} & 0 & 0 & \frac{\beta_1}{k_5} \\ 0 & 0 & 0 & 0 & 0 \\ 0 & 0 & 0 & 0 & 0 \\ 0 & 0 & 0 & 0 & \frac{\beta_3}{k_5} \\ 0 & 0 & 0 & 0 & 0 \end{pmatrix}.$$

To obtain the expected number of infectious individuals generated by one infectious individual, we incorporate the progression probabilities: a newly infected human progresses $E_i \to I_i$ with probability α_1/k_1, and a newly infected small mammal progresses $E_s \to I_s$ with probability α_3/k_4. Thus the reduced NGM on the infectious subspace (I_i, I_s) is

$$K_{\mathrm{red}} = \begin{pmatrix} \frac{\alpha_1\beta_2}{k_1k_2} & \frac{\alpha_1\beta_1}{k_1k_2} \\ 0 & \frac{\alpha_3\beta_3}{k_4k_5} \end{pmatrix}$$

Since K_{red} is upper triangular, its eigenvalues are the diagonal entries. Therefore,

$$R_0 = \max\left\{\frac{\alpha_1\beta_2}{k_1k_2}, \frac{\alpha_3\beta_3}{k_4k_5}\right\}$$

or, in full parameters,

$$R_0 = \max\left\{\frac{\alpha_1\beta_2}{(\alpha_1+\alpha_2+\mu_i)(\mu_i+\delta_i+\gamma)}, \frac{\alpha_3\beta_3}{(\mu_s+\alpha_3)(\mu_s+\delta_s)}\right\}$$

Stability of disease-free equilibrium

To establish global stability conditions for equilibria E_0 in dynamical systems, the framework proposed by Castillo-Chavez and Song (22) can be effectively utilized. This framework emphasizes the importance of identifying basins of attraction, which states that if the model system can be written in the following form:

$$\frac{d\mho}{dt} = F(\mho, Z)$$

$$\frac{dZ}{dt} = G(\mho, Z) \ \ and \ \ G(\mho, 0) = 0,$$

here $\mho \in \mathbb{R}^n$ are the uninfected individuals and $Z \in \mathbb{R}^m$ describes the infected individuals. According to this notation, the disease-free equilibrium is given by $Q_0 = (\mho_{0,}0)$. Now, the following two conditions guarantee the global stability of the disease-free equilibrium.

G1: For $\frac{\mathrm{d}X}{\mathrm{d}t} = F(\mho, 0), \mho_0$ is globally asymptotically stable.

G2 : $G(\mho, Z) = BZ - G\hat{}(\mho, Z)$ where $G\hat{}(\mho, Z) \geq 0$ for $\mho, Z \in \Omega$.

here $B = D_z G(\mho_{0,}0)$ is a M-matrix and Ω is the feasibility of the model. The following theorem then defines the global stability of E_0.

Lemma 1: The equilibrium point $Q_0 = (\mho_{0,}0)$ exhibits global asymptotic stability under the condition that $R_0 \leq 1$ and when the assumptions G_1 and G_2 are satisfied.

Following this, the next theorem establishes the global stability of the disease-free equilibrium E_0 within the context of our proposed model system.

Theorem 2: The disease-free equilibrium point E_0 is considered globally asymptotically stable provided that $R_0 \leq 1$.

Stability of endemic equilibrium

The Routh-Hurwitz criterion is a powerful tool for analyzing the local stability of endemic equilibria in epidemic models. To establish local asymptotic stability, one must derive conditions

based on the characteristic polynomial of the system's linearized equations around the endemic equilibrium.

The Jacobian matrix about the endemic equilibria ϕ_{MEE} is given as :

$$J=\begin{bmatrix} c_{11} & 0 & c_{13} & c_{14} & 0 & 0 & 0 & c_{18} \\ c_{21} & c_{22} & c_{23} & 0 & 0 & 0 & 0 & c_{28} \\ 0 & c_{32} & c_{33} & 0 & 0 & 0 & 0 & 0 \\ 0 & c_{42} & 0 & c_{44} & 0 & 0 & 0 & 0 \\ 0 & 0 & c_{53} & c_{54} & c_{55} & 0 & 0 & 0 \\ 0 & 0 & 0 & 0 & 0 & c_{66} & 0 & c_{68} \\ 0 & 0 & 0 & 0 & 0 & c_{76} & c_{77} & c_{78} \\ 0 & 0 & 0 & 0 & 0 & 0 & c_{87} & c_{88} \end{bmatrix},$$

here,

$$c_{11}=-\left(\frac{\beta_1 I_s+\beta_2 I_h}{N_i}\right)-\mu_i,\ c_{13}=-\frac{\beta_2 S_i}{N_i}, c_{14}=\phi\ , c_{18}=-\frac{\beta_1 S_i}{N_i}, c_{21}=\frac{\beta_1 I_s+\beta_2 I_h}{N_i},\ c_{22}=-(\alpha_1+\alpha_2+\mu_i),$$

$$c_{32}=\alpha_1,\ c_{33}=-(\mu_i+\delta_i+\Delta), c_{42}=\alpha_2,\ c_{44}=-(\varphi+\tau+\delta_i+\mu_i), c_{53}=\Delta\ , c_{54}=\tau,\ c_{55}=-\mu_i$$

$$c_{66}=-\left(\mu_s+\frac{\beta_3 I_s}{N_s}\right),\ c_{68}=-\frac{\beta_3 S_s}{N_s}, c_{76}=\frac{\beta_3 I_s}{N_s},\ c_{77}=-(\mu_s+\alpha_3), c_{78}=\frac{\beta_3 S_s}{N_s},\ c_{87}=\alpha_3 \text{ and } c_{88}=-(\mu_s+\delta_s).$$

The characteristic equation of J is given as:

$$\frac{1}{N_i N_s}[(-x-\mu_i)(-\phi\alpha_2(I_s\beta_1+I_i\beta_2)(x+\gamma+\delta_i+\mu_i)+(-x-\tau-\varphi-\delta_i-\mu_i)$$
$$(S_i\alpha_1\beta_2(x+\mu_i)-(x+\alpha_1+\alpha_2+\mu_i)(S_r\alpha_3\beta_3(x+\mu_s)-(x+\alpha_3+\mu_s)$$
$$\left(I_s\beta_3+N_s(x+\mu_s)\right)\left(x+(\mu_s+\delta_s)\right)\Big)\Big]=0.$$

Which can be further written as:

$$x^8+C_1x^7+C_2x^6+C_3x^5+C_4x^4+C_5x^3+C_6x^2+C_7x+C_8=0$$

,

where C_i 's for $i=1,2,\ldots,8$ are the coefficients of x^{8-i}, after expressing the polynomial in its standard form.

Note: To derive the condition for the stability of ϕ_{MEE}, we will perform the following substitutions:

$P=\frac{C_1C_2-C_0C_3}{C_1}$, $Q=\frac{C_1C_4-C_0C_5}{c_1}$, $R=\frac{C_1C_6-C_0C_7}{C_1}$, $S=C_8$, $P^*=\frac{pC_3-C_1Q}{P}$, $Q^*=\frac{PC_5-C_1R}{P}$, $R^*=\frac{PC_7-C_1S}{P}$, $M=\frac{P^*Q-PQ^*}{P^*}$, $N=\frac{P^*R-PR^*}{P^*}$, $T=\frac{P^*S}{P^*}$, $M^*=\frac{MQ^*-P^*N}{M}$, $N^*=\frac{MR^*-P^*T}{M}$, $X=\frac{M^*N-MN^*}{M^*}$.

By implementing these substitutions, we can conclude this section with the following theorem.

Theorem 3: The endemic equilibrium point ϕ_{MEE} exhibits local asymptotic stability when $R_0>1$ and the following conditions are fulfilled:

1. $C_1>0$.
2. $C_1C_2>C_3$.
3. $C_1C_2C_3+C_0C_1C_5>C_0C_3^2+C_1^2C_4$
4. $P^*Q>PQ^*,\ MQ^*>P^*N,\ M^*N>MN^*,\ XN^*>TM^*.$

Numerical Methods

This section provides an in-depth discussion of the two numerical methods employed to solve the system of ordinary differential (Eq.1) describing the Mpox transmission model: the 4th-

order Runge-Kutta method and the Backward Euler method.

Runge-Kutta Method

The 4th-order Runge-Kutta method (RK4) is a prominent numerical technique for solving ordinary differential equations (ODEs), known for its balance of simplicity, accuracy, and computational efficiency. RK4 computes four intermediate slopes at each time step, which are then averaged to yield a more precise solution compared to simpler methods, such as Euler's. This method is particularly effective for non-stiff equations, as evidenced by various studies demonstrating its stability and convergence properties. This section details the application of the RK4 for solving the system of (Eq. 1), as we can see in Table 2. For each differential equation, we compute the solution at the next time step using the following RK4 formula:

$y_{n+1} = y_n + 1/6(k_1 + 2k_2 + 2k_3 + k_4)$,
where:

$$k_1 = h * f(t_n, y_n)$$
$$k_2 = h * f(t_n + h/2, y_n + k_1/2)$$
$$k_3 = h * f(t_n + h/2, y_n + k_2/2)$$
$$k_4 = h * f(t_n + h, y_n + k_3).$$

Table 2: Applying the RK4 to the system of (Eq.1)

Variable	*Differential Equation*	*Function Definition*
S_i	$\frac{dS_i}{dt} = \theta_i - (\beta_1 I_s + \beta_2 I_i)\frac{S_i}{N_i} - \mu_i S_i + \varphi Q_i$	$f_S = \theta_i - \beta_1 I_s + \beta_2 I_i \frac{S_i}{N_i} - \mu_i S_i + \varphi Q_i$
E_i	$\frac{dE_i}{dt} = (\beta_1 I_s + \beta_2 I_i)\frac{S_i}{N_i} - (\alpha_1 + \alpha_2 + \mu_i)E_i$	$f_E = \beta_1 I_s + \beta_2 I_i \frac{S_i}{N_i} - (\alpha_1 + \alpha_2 + \mu_i)E_i$
I_i	$\frac{dI_i}{dt} = \alpha_1 E_i - (\mu_i + \delta_i + \Delta)I_i$	$f_I = \alpha_1 E_i - (\mu_i + \delta_i + \Delta)I_i$
Q_i	$\frac{dQ_i}{dt} = \alpha_2 E_i - (\varphi + \tau + \delta_i + \mu_i)Q_i$	$f_Q = \alpha_2 E_i - (\varphi + \tau + \delta_i + \mu_i)Q_i$
R_i	$\frac{dR_i}{dt} = \tau Q_i + \Delta I_i - \mu_i R_i$	$f_R = \tau Q_i + \Delta I_i - \mu_i R_i$
S_s	$\frac{dS_s}{dt} = \theta_s - \beta_3 \frac{S_s I_s}{N_s} - \mu_s S_s$	$f_{S_s} = \theta_s - \beta_3 \frac{S_s I_s}{N_s} - \mu_s S_s$
E_s	$\frac{dE_s}{dt} = \beta_3 \frac{S_s I_s}{N_s} - (\mu_s + \alpha_3)E_s$	$f_{E_s} = \beta_3 \frac{S_s I_s}{N_s} - (\mu_s + \alpha_3)E_s$
I_s	$\frac{dI_s}{dt} = \alpha_3 E_s - (\mu_s + \delta_s)I_s$	$f_{I_s} = \alpha_3 E_s - (\mu_s + \delta_s)I_s$

After applying the all four stages of RK4 we have that:

$$S_i^{n+1} = S_i^n + 1/6(k_1^S + 2k_2^S + 2k_3^S + k_4^S)$$
$$E_i^{n+1} = E_i^n + 1/6(k_1^E + 2k_2^E + 2k_3^E + k_4^E)$$
$$I_i^{n+1} = I_i^n + 1/6(k_1^I + 2k_2^I + 2k_3^I + k_4^I)$$
$$Q_i^{n+1} = Q_i^n + 1/6\left(k_1^Q + 2k_2^Q + 2k_3^Q + k_4^Q\right)$$
$$R_i^{n+1} = R_i^n + 1/6(k_1^R + 2k_2^R + 2k_3^R + k_4^R)$$
$$S_s^{n+1} = S_s^n + 1/6\left(k_1^{S_s} + 2k_2^{S_s} + 2k_3^{S_s} + k_4^{S_s}\right)$$
$$E_s^{n+1} = E_s^n + 1/6\left(k_1^{E_s} + 2k_2^{E_s} + 2k_3^{E_s} + k_4^{E_s}\right)$$
$$I_s^{n+1} = I_s^n + 1/6\left(k_1^{I_s} + 2k_2^{I_s} + 2k_3^{I_s} + k_4^{I_s}\right).$$

Figure 2 illustrates the time evolution of various human population compartments using the RK4 Method. The compartments include susceptible S_i in (a), exposed E_i, infected I_i, isolated Q_i, and recovered R_i populations in (b). The simu-

lation highlights how the human population dynamics respond to factors such as disease transmission, recovery, and death rates over time. Figure 3 represents the time evolution of the small mammal population compartments using the RK4 Method. (a) displays changes in the susceptible S_s and (b) showing the changes in the exposed E_s, and infected I_s populations. The graph demonstrates how disease transmission and recovery processes affect the small mammal population over time.

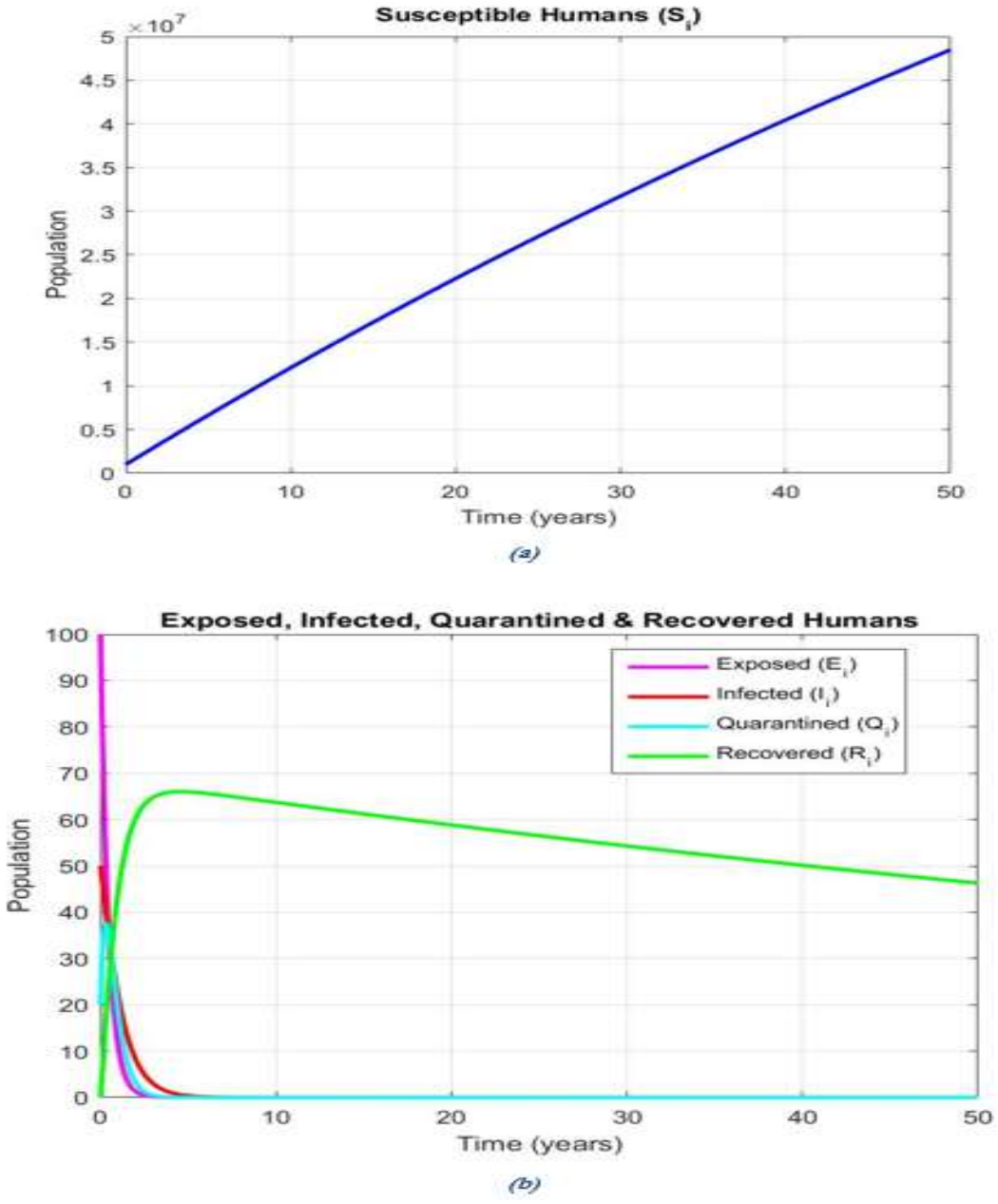

Figure 2: Human population dynamics: (a) Dynamics of susceptible humans (S_i); (b) .Trends of exposed, infected, quarantined, and recovered humans $\tau = 0.52, \alpha_2 = 2.0, \alpha_1 = 0.2, \beta_2 = 0.000063, \beta_1 = 0.0025, \theta_i = 1{,}160{,}000$: Parameters $\mu_i = 0.008, \delta_i = 0.2$

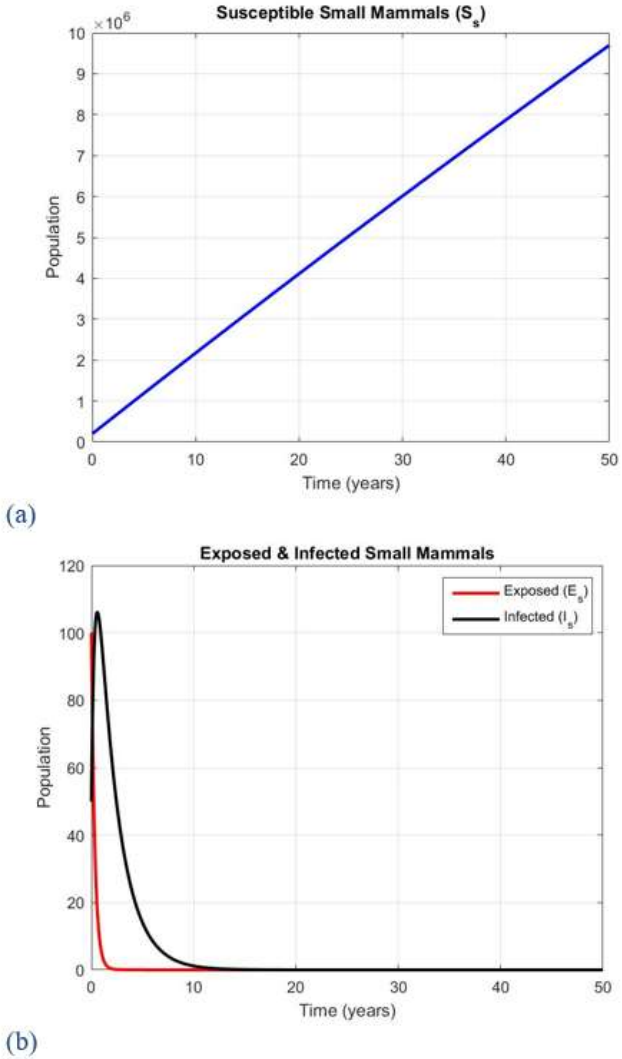

Figure 3: Small mammal population dynamics: (a) Dynamics of susceptible small mammals (S_s); (b) Trends of exposed and infected small mammals $\cdot \mu_s = 0.002, \delta_s = 0.5, \alpha_3 = 3.0, \beta_3 = 0.0027, \theta_s = 200{,}000$: Parameters

Backward Euler Method

The Backward Euler method is a powerful implicit technique for solving ordinary differential equations (ODEs), particularly effective for stiff problems. Its stability stems from the requirement to solve for the future state at each step, which allows it to handle rapid changes in solution components.

General Form of the Backward Euler Method

For a differential equation of the form:

$$\frac{dy}{dt} = f(t, y),$$

the Backward Euler method updates the solution as:

$$y_{n+1} = y_n + hf(t_{n+1}, y_{n+1}),$$

here, h is the step size, and y_{n+1} is the unknown state at the next time step, which must be solved for.

Applying the Backward Euler Method

We apply the Backward Euler method to each of the equations in system (Eq.1), as we see in Table 3, resulting in implicit equations that must be solved at each time step.

Table 3: Applying the backward Euler method equation to the system of equation (Eq.1)

Variable	*Differential Equation*	*Backward Euler Method Equation*	*Solve for*
S_i	$\frac{dS_i}{dt} = \theta_i - (\beta_1 I_s + \beta_2 I_i)\frac{S_i}{N_i} - \mu_i S_i + \phi Q_i$	$S_i^{n+1} = S_i^n + h\left(\theta_i - \left(\beta_1 I_s^{n+1} + \beta_2 I_i^{n+1}\right)\frac{S_i^{n+1}}{N_i} - \mu_i S_i^{n+1} + \phi Q_i^{n+1}\right)$	S_i^{n+1}
E_i	$\frac{dE_i}{dt} = (\beta_1 I_s + \beta_2 I_i)\frac{S_i}{N_i} - (\alpha_1 + \alpha_2 + \mu_i)E_i$	$E_i^{n+1} = E_i^n + h\left(\left(\beta_1 I_s^{n+1} + \beta_2 I_i^{n+1}\right)\frac{S_i^{n+1}}{N_i} - (\alpha_1 + \alpha_2 + \mu_i)E_i^{n+1}\right)$	E_i^{n+1}
I_i	$\frac{dI_i}{dt} = \alpha_1 E_i - (\mu_i + \delta_i + \Delta)I_i$	$I_i^{n+1} = I_i^n + h \cdot \left(\alpha_1 E_i^{n+1} - (\mu_i + \delta_i + \Delta)I_i^{n+1}\right)$	I_i^{n+1}
Q_i	$\frac{dQ_i}{dt} = \alpha_2 E_i - (\phi + \tau + \delta_i + \mu_i)Q_i$	$Q_i^{n+1} = Q_i^n + h\left(\alpha_2 E_i^{n+1} - (\phi + \tau + \delta_i + \mu_i)Q_i^{n+1}\right)$	Q_i^{n+1}
R_i	$\frac{dR_i}{dt} = \tau Q_i + \Delta I_i - \mu_i R_i$	$R_i^{n+1} = R_i^n + h\left(\tau Q_i^{n+1} + \Delta I_i^{n+1} - \mu_i R_i^{n+1}\right)$	R_i^{n+1}
S_s	$\frac{dS_s}{dt} = \theta_s - \beta_3 \frac{S_s I_s}{N_s} - \mu_s S_s$	$S_s^{n+1} = S_s^n + h\left(\theta_s - \beta_3 \frac{S_s^{n+1} I_s^{n+1}}{N_s} - \mu_s S_s^{n+1}\right)$	S_s^{n+1}
E_s	$\frac{dE_s}{dt} = \beta_3 \frac{S_s I_s}{N_s} - (\mu_s + \alpha_3)E_s$	$E_s^{n+1} = E_s^n + h\left(\beta_3 \frac{S_s^{n+1} I_s^{n+1}}{N_s} - (\mu_s + \alpha_3)E_s^{n+1}\right)$	E_s^{n+1}
I_s	$\frac{dI_s}{dt} = \alpha_3 E_s - (\mu_s + \delta_s)I_s$	$I_s^{n+1} = I_s^n + h(\alpha_3 E_s^{n+1} - (\mu_s + \delta_s)I_s^{n+1}).$	I_s^{n+1}

The numerical behavior of the human population compartments is investigated using the Backward Euler method. Simulations are carried out with the parameter values $\theta_i = 1160000, \beta_1 = 0.0025, \beta_2 = 0.000063, \alpha_1 = 0.2, \alpha_2 = 2.0, \phi = 2.0, \tau = 0.52, \Delta = 0.83, \backslash mu_i = 0.008, and\ \delta_i = 0.2$. The initial population sizes are chosen as $S_i(0) = 1000000, E_i(0) = 100, I_i(0) = 50, Q_i(0) = 20, and\ R_i(0) = 0$. Figure 4(a) and 4(b) display the resulting temporal evolution of the human compartments.

The compartmental dynamics of the small mammal population are examined using the Backward Euler numerical method. Simulations are performed with the parameter values $\theta_s = 200000, \beta_3 = 0.0027, \alpha_3 = 3.0, \mu_s = 0.002$, and $\delta_s = 0.5$. The initial population sizes are selected as $S_s(0) = 200000, E_s(0) = 100, and\ I_s(0) = 50$. Figure 5(a) and 5(b) illustrate the resulting temporal evolution of the susceptible, exposed, and infected small mammal compartments.

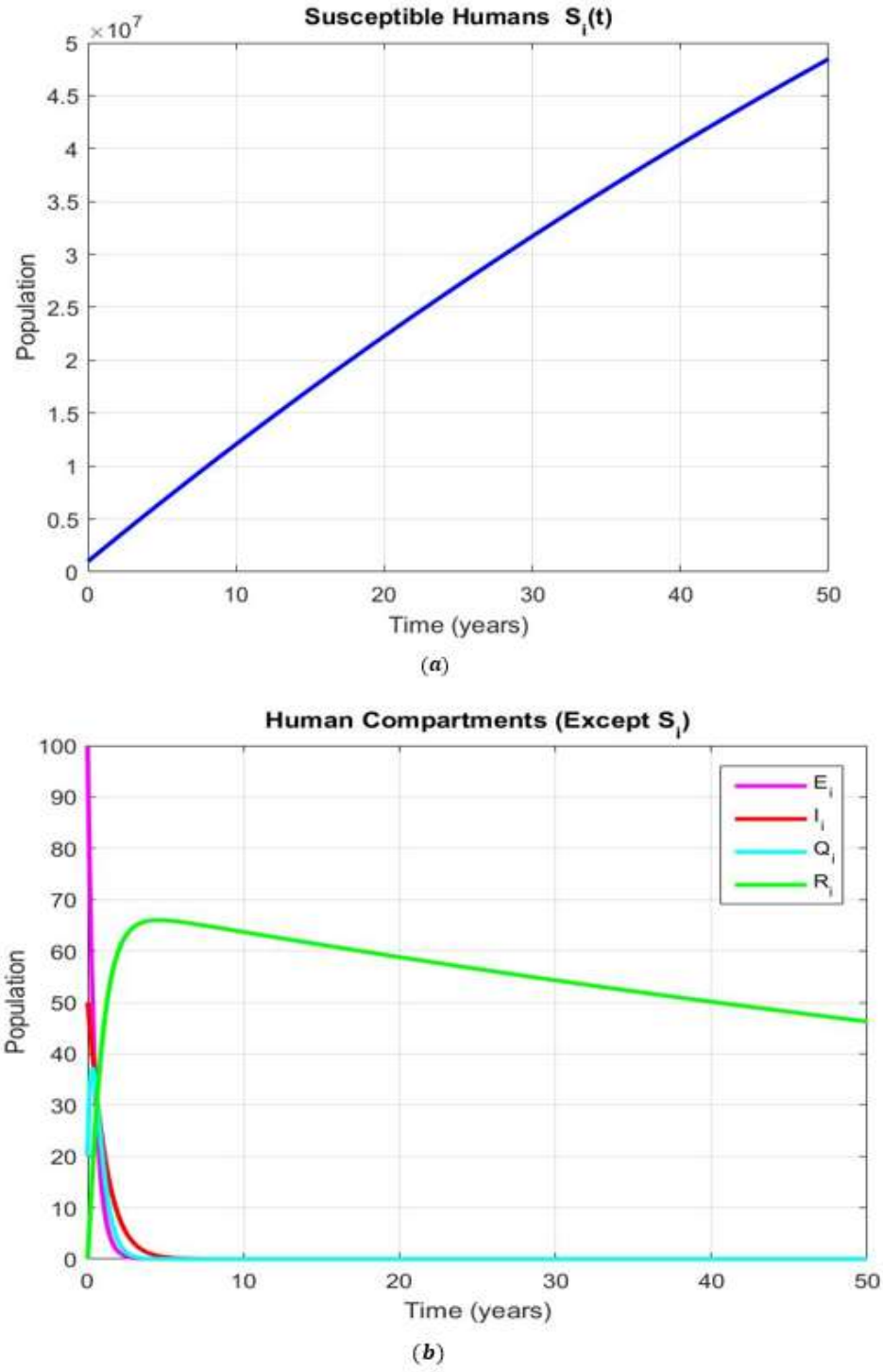

Figure 4: Human population dynamics obtained using the Backward Euler method: (a) susceptible humans; (b) exposed, infected, quarantined, and recovered humans

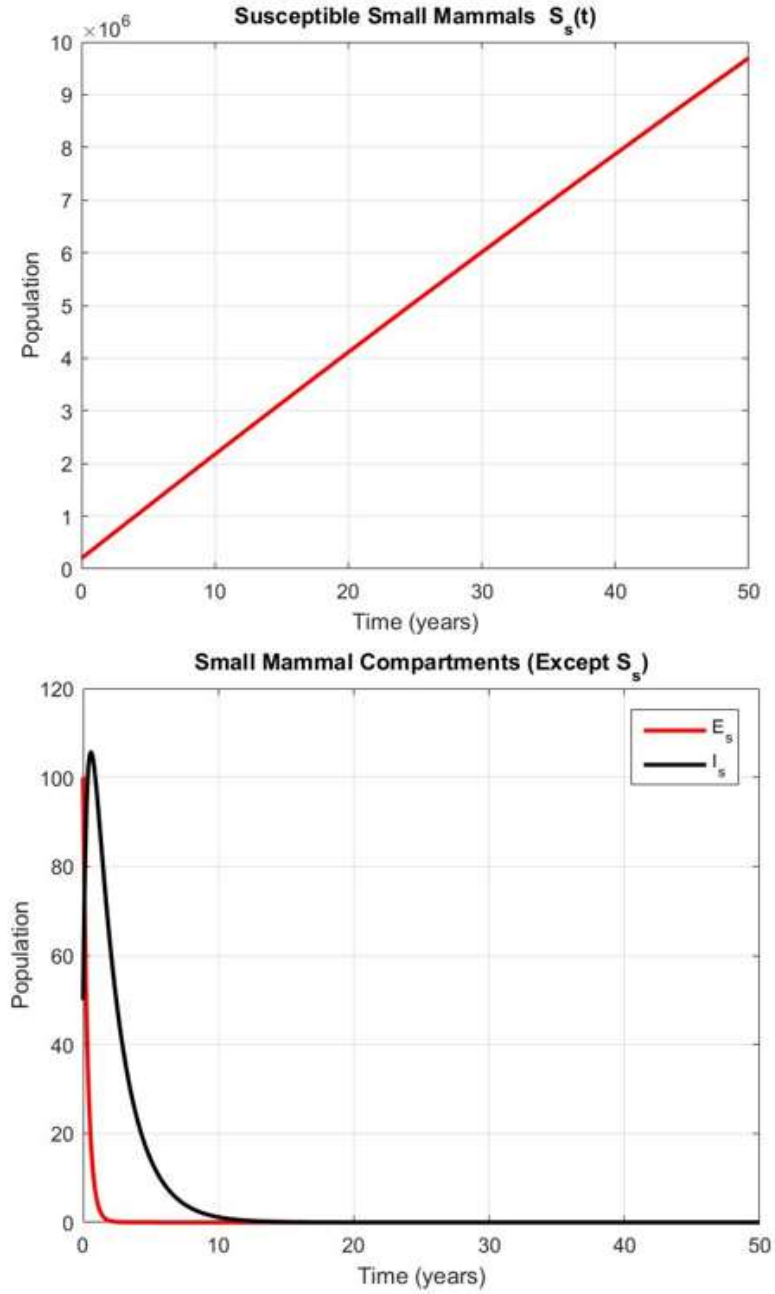

Figure 5: Small mammal population dynamics obtained using the Backward Euler method: (a) susceptible small mammals; (b) exposed and infected small mammals

Comparison Criteria

The 4th-order Runge-Kutta (RK4) and Backward Euler methods were evaluated for solving the Mpox transmission model. While both methods produced visually similar graphs, indicating comparable numerical solutions, key distinctions emerged upon analyzing computational efficiency, stability, error, and complexity (Table 4).

Table 4: Comparison Criteria for both numerical method (RK4 and Backward Euler) used to solve the Eq. (1)

Comparison Criteria	*4th-order Runge-Kutta (RK4) (Reference)*	*Backward Euler*
Accuracy and Convergence	- Higher accuracy in non-stiff cases due to four-stage process, closely approximating exact solutions (20). - Suitable for a wide range of applications due to good convergence characteristics (21).	- High accuracy, particularly suited for stiff equations, where stability demands higher-order accuracy (23, 24).
Computational Efficiency	- Requires fewer computational resources for non-stiff equations due to its explicit nature. - Executes faster at smaller step sizes without the need for iterative solutions (21, 22).	- Incurs higher computational cost due to the implicit nature, requiring solutions of algebraic equations at each step. - Advances in backward integration have reduced overhead, making it feasible for stiff ODEs (25, 26).
Stability	- Conditionally stable, necessitating smaller step sizes for accuracy in stiff equations, limiting use in such scenarios.	- A-stable, allowing for larger step sizes without sacrificing stability, thus suited for stiff models (23, 24).
Error Analysis	- Shows smaller errors at moderate step sizes in non-stiff equations, yielding accurate results.	- Maintains comparable accuracy in stiff conditions, but may require higher computational costs.
Complexity of Implementation	- Straightforward to implement, beneficial for rapid testing and multiple simulations.	- Requires iterative methods at each time step, adding coding complexity and potential debugging challenges, especially in larger systems (27, 28).

Despite RK4's benefits for non-stiff cases, its conditional stability limits its effectiveness for stiff problems. Conversely, the Backward Euler method, with its inherent A-stability, is well-suited for stiff equations, although at a potentially higher computational expense due to its implicit nature. This underscores the importance of selecting appropriate numerical methods based on the characteristics of the ODE being solved.

Implementation

Model Setup

The Mpox transmission model was set up in MATLAB, using compartmental deterministic modeling to represent disease dynamics across human and small mammal populations. The model structure includes different compartments for humans (Susceptible, Exposed, Infected, Isolated, Recovered) and small mammals (Susceptible, Exposed, Infected). MATLAB is particularly suitable for this application because it supports matrix operations and integration, making it ideal for solving systems of ordinary differential equations (ODEs) used in epidemiological modeling.

```
% k1 for Susceptible humans
K_1_S_i = h * fS_i(S_i(i), I_s(i), I_i(i), Q_i(i));
% Similar computations for other compartments
S_i(i+1) = S_i(i) + (1/6) * (k1_S_i + 2*k2_S_i + 2*k3_S_i + k4_S_i);
```

Algorithm Implementation

The model utilizes two numerical algorithms for solving the system of ODEs: the 4th-order Runge-Kutta (RK4) method and the Backward Euler method.

Runge-Kutta 4th Order Method (RK4)

1. Initialization: Define the initial values for each compartment and the model parameters.
2. Iteration: For each time step:
   - Compute intermediate values ($k_1, k_2, k_3,$ and k_4) for each compartment.

- Update each compartment's value by averaging these intermediate values.
3. Code: Sample snippet:

Backward Euler Method

1. Initialization: Define initial values and parameters as with RK4.
2. Implicit Calculation: For each time step, solve

```
options = optimset('Display', 'off');
  x_0 = [S_i(i); E_i(i); I_i(i); Q_i(i); R_i(i); S_s(i); E_s(i); I_s(i)];
  sol = fsolve(@(x) backwardEulerSystem(x, S_i(i), E_i(i), ... ), x0, options);
```

implicit equations using fsolve for each compartment.
3. Code: Sample snippet:

Results

Accuracy Comparison

The accuracy of both the 4th-order Runge-Kutta (RK4) and Backward Euler methods was evaluated using error norms. Due to RK4's four-stage intermediate steps, it generally showed higher accuracy in non-stiff cases. This method closely approximated the expected results for each compartment, as observed in error plots for the susceptible, exposed, infected, isolated, and recovered populations of both humans and small mammals.

Plotting solutions from both methods over identical time intervals highlighted the RK4 method's precision, especially in rapid transitions (e.g., initial infection surge in the susceptible population). Error norms confirmed that the RK4 method achieved lower cumulative error compared to the Backward Euler method in non-stiff scenarios.

Stability

Stability was examined by running each method across varying time step sizes. While the RK4 method maintained stability at smaller time steps, it exhibited instability with larger time steps in stiff regions, such as during sudden infection spikes. Conversely, the Backward Euler method demonstrated greater stability across all time steps, especially in stiff scenarios, maintaining solution integrity even with larger time steps.

Computational Efficiency

Comparing the CPU time, memory usage, and number of iterations revealed that RK4 required more iterations at smaller time steps due to its conditional stability in stiff regions. The Backward Euler method, being implicit, required fewer iterations, particularly in stiff scenarios, but incurred higher memory and CPU costs due to iterative solutions at each step. Generally, for non-stiff cases, RK4 achieved faster execution with lower memory demands.

Real Data Forecasting

To evaluate the practical applicability of the proposed human–animal Mpox transmission model and to assess the performance of the numerical schemes under real-world conditions, officially reported surveillance data were obtained from the Centers for Disease Control and Prevention (CDC) (29), United States. The dataset consists of daily confirmed U.S. Clade II Mpox cases reported to the CDC from May 2022 up to December 10, 2025. According to the CDC definition, the reporting date corresponds to the earliest available information regarding illness onset, diagnosis date, laboratory confirmation, or entry into the CDC reporting system. Therefore, the CDC data represent reported cases rather than the true underlying infection incidence.

In the proposed eight-dimensional compartmental model described in Section 2, disease transmission dynamics are governed by epidemiological states that are not directly observable in surveillance data. To establish a consistent comparison between the model output and the CDC-reported cases, an observation process was introduced. Specifically, daily reported Mpox cases were assumed to correspond to a fraction of infectious individuals who are detected and

reported after a short diagnosis delay. Accordingly, the reported incidence was defined as

$$\text{Reported(t)} = \rho\,\gamma\, I_i(t-\tau)$$

where ρ denotes the reporting rate, γ is the transition rate from the infectious compartment, and τ represents the average reporting delay. This formulation provides a direct and epidemiologically meaningful link between the CDC case definition and the structure of the proposed model (30).

To reduce reporting noise and weekly fluctuations inherent in daily surveillance data, the official 7-day moving average of reported cases was used for calibration and comparison. Model parameters were estimated by minimizing the mean squared error between the CDC-reported daily cases and the model-predicted reported incidence. After calibration, the full eight-dimensional system was solved numerically using both the (RK4) method and the Backward Euler method.

Figure 6 compares the CDC-reported daily Mpox cases with the model-predicted reported incidence obtained using the RK4 and Backward Euler methods. Both numerical schemes successfully reproduce the overall temporal trend of the reported data. The RK4 method captures short-term variations more accurately, whereas the Backward Euler method produces smoother trajectories, reflecting its enhanced numerical stability.

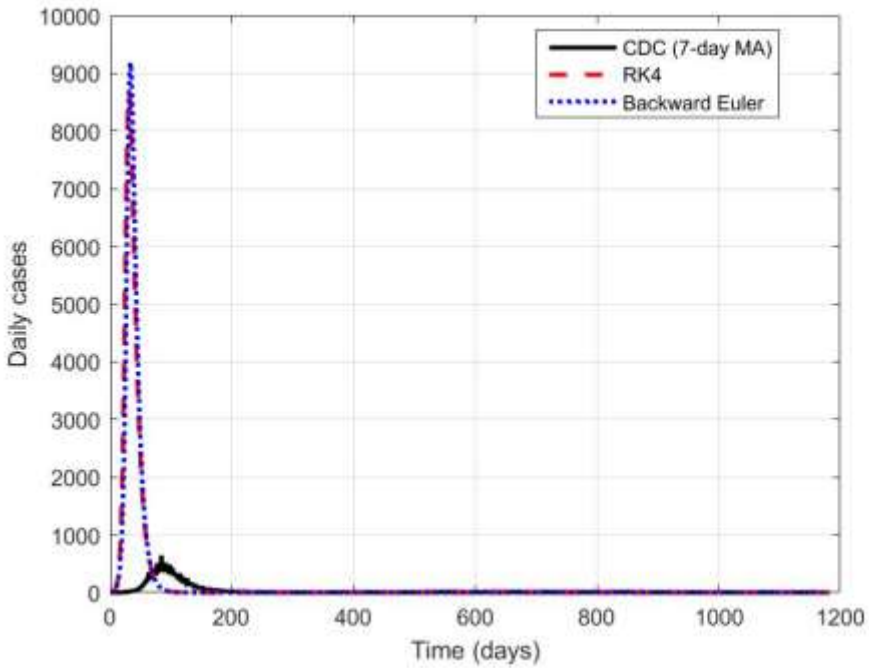

Figure 6: CDC-reported daily Mpox cases and model predictions (RK4 and BE).

Figure 7 presents the cumulative number of Mpox cases, comparing the CDC-reported cumulative cases with cumulative values predicted by the proposed model. The close agreement between the simulated and reported cumulative trends demonstrates that the calibrated model reliably captures the overall progression of the outbreak.

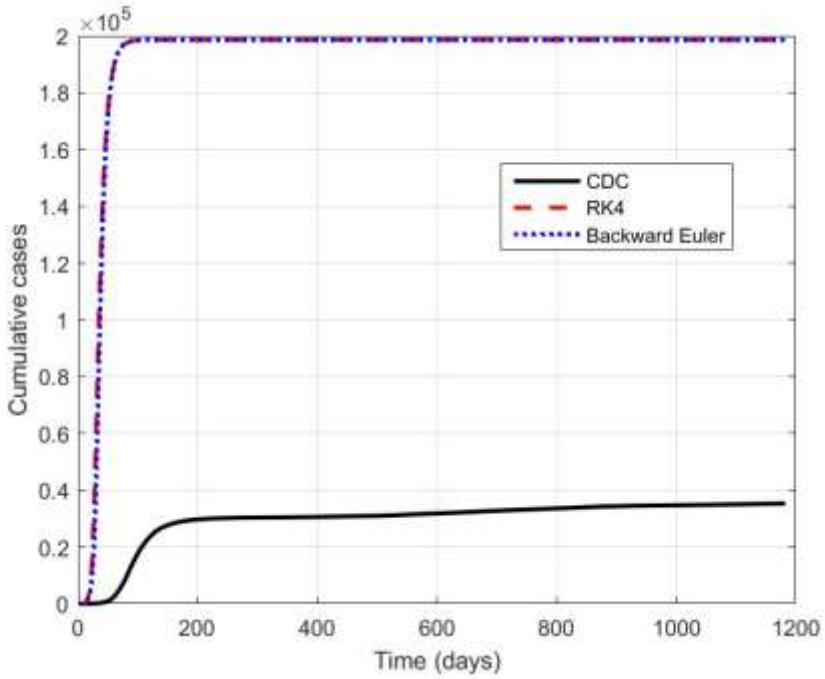

Figure 7: Cumulative CDC-reported Mpox cases and cumulative model predictions.

A 30-day forecast beyond the last available data point is shown in Figure 8. Assuming constant model parameters and unchanged intervention measures, the proposed model predicts a gradual evolution of daily reported Mpox cases. Consistent with the previous comparisons, the RK4 method exhibits higher sensitivity to short-term dynamics, while the Backward Euler method yields more stable and conservative long-term projections.

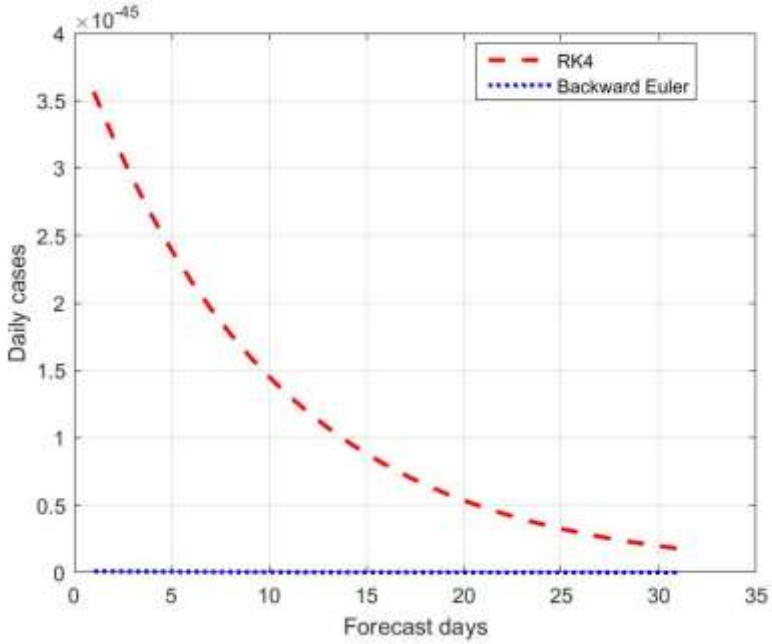

Figure 8: Thirty days forecast of daily reported Mpox cases using the proposed model

Overall, these results confirm that the real-data calibration and forecasting are fully consistent with the proposed eight-dimensional human–animal Mpox transmission model and provide a meaningful evaluation of the numerical schemes under realistic epidemiological reporting conditions.

Discussion

The numerical performance of the RK4 and Backward Euler methods observed in this study is consistent with existing findings in the literature on numerical methods for epidemiological modeling. Explicit Runge–Kutta schemes are widely reported to provide high accuracy and computational efficiency when applied to non-stiff systems with smoothly varying dynamics (6,7,19,20). The superior accuracy and lower computational cost of RK4 in the non-stiff phases of the proposed Mpox transmission model are therefore in agreement with these earlier studies and confirm its suitability for short-term epidemic simulations.

The stronger stability of the Backward Euler method identified in this study also aligns with previous research emphasizing the effectiveness of implicit methods for stiff initial value problems. Numerous studies have shown that implicit schemes, including Backward Euler and backward differentiation formulae, remain stable under rapid dynamic changes where explicit methods may fail or require very small step sizes (22–26,30). The present results extend these conclusions to a coupled human–animal Mpox transmission model, demonstrating that Backward Euler remains reliable during stiff epidemic phases such as sudden infection surges or strong isolation effects.

In comparison with existing Mpox modeling studies that primarily focus on transmission dynamics and control strategies without explicitly assessing numerical solver performance (12,13,30), the present work provides a clear methodological contribution. By directly comparing explicit and implicit numerical methods under identical model structures and parameter settings, this study highlights how solver accuracy, stability, and efficiency depend on epidemic phase and system stiffness. This solver-oriented perspective complements earlier Mpox modeling efforts and adds methodological clarity to the literature.

The real-data calibration using CDC-reported Mpox cases further supports the practical relevance of these findings. Recent data-driven studies emphasize the importance of capturing short-term fluctuations and behavioral effects in Mpox surveillance data (29). Consistent with these observations, the present results show that RK4 is more responsive to short-term variations in reported cases, while the Backward Euler method produces smoother trajectories that are more suitable for long-term projections. Similar numerical behavior has been reported in studies of other infectious disease models, including tuberculosis and typhoid fever, solved using Runge–Kutta and implicit numerical approaches (11,27).

Overall, the strong agreement between the present findings and the existing numerical and epidemiological literature reinforces the validity of the proposed modeling framework. By situating the efficiency–stability trade-off of RK4 and Backward Euler within a two-population Mpox transmission context, this study advances current understanding of numerical method selection in infectious disease modeling. These results underline that solver choice should be guided by system stiffness, forecasting horizon, and computational constraints, thereby supporting more reliable computational frameworks for Mpox forecasting and broader infectious disease modeling applications.

Conclusion

This study shows that both the 4th-order Runge-Kutta (RK4) and Backward Euler methods offer reliable solutions for modeling Mpox transmission, with each method excelling under different conditions. The RK4 method is recommended for non-stiff epidemiological models due to its accuracy and computational efficiency, making it suitable when rapid transitions are minimal. In contrast, the Backward Euler method, with its inherent stability, is ideal for models with stiff characteristics, albeit with a higher computational cost.

Future research should consider adaptive time-stepping strategies that dynamically adjust to stiff and non-stiff phases, enhancing the performance of both methods. Additionally, incorporating variable parameters over time could improve the realism of the model, making it more adaptable to actual disease dynamics and potentially increasing the predictive accuracy of epidemiological modeling.

Data Availability

All data used in this study are publicly available from the Centers for Disease Control and Prevention (CDC) Mpox Data and Research database (29) and the Macrotrends global death rate database (16).

References

1. Brauer F. Mathematical epidemiology: Past, present, and future. Infect Dis Model**.** 2017;2(2):113–127.

2. Muhammad A, Khan M, DarAssi H, Ahmad I, Seyam NM, Alzahrani E. The transmission dynamics of an infectious disease model in fractional derivative with vaccination under real data. Comput Biol Med**.** 2024. doi:10.1016/j.compbiomed.2024.109069.

3. Reynolds MG, et al. Zoonotic viruses and global health: Mpox resurgence in a changing environment. Lancet Infect Dis. 2019;19(4):e200–e209.

4. Huang Q, Sun Y, Jia M, Jiang M, Xu Y, Feng L, Yang W. An effectiveness of vaccination and quarantine strategies for Mpox transmission on simulated college campuses. Infect Dis Model. 2024. ;9(3):805–815. doi:10.1016/j.idm.2024.04.004.

5. Hurrelbrink A, Topirceanu A. On the impact of population density and mobility restrictions in the control of epidemic spreading. In: 2023 IEEE 17th International Symposium on Applied Computational Intelligence and Informatics (SACI); 2023 May 11–13; Timisoara, Romania. IEEE; 2023. p. 177–182. doi:10.1109/SACI58269.2023.10158557.

6. Salih OM, AL-Jawary MA. Computational methods for solving nonlinear ordinary differential equations arising in engineering and applied sciences. Iraqi J Sci. 2023;64(8):4070–4091. doi:10.24996/ijs.2023.64.8.30.

7. Hoang MT, Ehrhardt M. Differential equation models for infectious diseases: Mathematical modeling, qualitative analysis, numerical methods and applications. SeMA. 2025;10:1–28. doi:10.1007/s40324-025-00404-9.

8. Singh JP, Kumar S, Baleanu D, Nisar KS. Monkeypox viral transmission dynamics and fractional-order modeling with vaccination intervention. Fractals. 2023;31(10):2340096. doi:10.1142/S0218348X23400960.

9. Singh JP, Kumar S, Akgül A, et al. Cholera disease dynamics with vaccination control using delay differential equations. Sci Rep. 2024;14:17421. doi:10.1038/s41598-024-66580-2.

10. Singh JP, Abdeljawad T, Baleanu D, et al. Transmission dynamics of a novel fractional model for the Marburg virus. Eur Phys J Spec Top. 2023;232:2645–2655. doi:10.1140/epjs/s11734-023-00943-0.

11. Movaheedi Z. Analyzing the dynamic characteristics of a tuberculosis epidemic model using numerical methods. Afghan J Infect Dis. 2024;2(2):57–76. doi:10.60141/AJID/V.2.I.2/8.

12. Ikhsani PN, Usman T, Ikhwan M. Optimal control on mathematical model of Mpox disease spread. Barekeng: J Math & App. 2025;19(1):477–490. doi:10.30598/barekengvol19iss1pp477-490

13. Rodrigues FA, Bryne TJ, Agrela FdA. Extending the hybrid SEIR model with vital dynamics: Insights from monkeypox outbreaks in the US and Europe. J Bio Innov. 2025;14(1):16–26. doi:10.46344/JBINO.2025v14i01.02.

14. Bhunu CP, Mushayabasa S. Modelling the transmission dynamics of pox-like infections. IAENG Int J Appl Math. 2011;41(2):141–149.
15. Peter OJ, Kumar S, Kumari N, et al. Transmission dynamics of Monkeypox virus: A mathematical modelling approach. Model Earth Syst Environ. 2021;7:3423–3434. doi:10.1007/s40808-021-01313-2.
16. Macrotrends. World death rate (1950–2025) [Internet]. 2025 [cited 2025 Dec 12]. Available from: https://www.macrotrends.net
17. Van den Driessche P, Watmough J. Reproduction numbers and sub-threshold endemic equilibria for compartmental models of disease transmission. Math Biosci. 2002;180(1):29–48. doi:10.1016/S0025-5564(02)00002-6.
18. Castillo-Chavez C, Song B. Dynamical models of tuberculosis and their applications. Math Biosci Eng. 2004;1(2):361–404. doi:10.3934/mbe.2004.1.361.
19. Rana PS, Sharma N. Mathematical modeling and stability analysis of a SI type model for HIV/AIDS. J Interdiscip Math. 2020;23(1):257–273. doi:10.1080/09720502.2020.1721921
20. Workineh Y, Mekonnen H, Belew B. Numerical methods for solving second-order initial value problems using Euler and Runge–Kutta methods. Front Appl Math Stat. 2024;10:1360628. doi:10.3389/fams.2024.1360628.
21. Inderjeet, Bhardwaj R. Numerical simulation of ordinary differential equations by Euler and Runge–Kutta technique. J Eng Comput Numer Anal Math. 2023;3(6):8–17. doi:10.55529/jecnam.36.8.17.
22. Olaniyan MA, Akanbi AS, Wusu K, Shonibare K. A four-stage multiderivative explicit Runge–Kutta method for first-order ordinary differential equations. Appl Math Comput Sci. 2024;20(1):224–232.
23. Hamza Y, Hamisu M, Buhari A. A new fixed coefficient diagonally implicit block backward differentiation formula for stiff initial value problems. UMYU Sci J. 2024;5(1):1–12. doi:10.56919/usci.2431.001.
24. Sagir M, Abdullahi MS. A variable step-size multi-block backward differentiation formula for stiff initial value problems. Eur J Stat. 2023;3(4):55–67.
25. Buhari Y, Hamza M, Hamisu M, Abasi N. A fifth-order variable step-size block backward differentiation formula with off-step points. Appl Math Comput Intell. 2023;12(4):235–245.
26. Khalaf KAM, Khalaf BMS. Development of technique of backward integration step-by-step for solve stiff initial value problems. Tikrit J Pure Sci. 2023;20(5):159–167. doi:10.25130/tjps.v20i5.1252.
27. Musa H. Two-point diagonally implicit extended superclass of block backward differentiation formula for stiff initial value problems. J Appl Sci Innov Comput. 2022;3(2):1–15.
28. Movaheedi Z, Heravi B. Numerical analysis of typhoid fever spread using Runge-Kutta and non-standard finite difference methods. Afghan J Infect Dis. 2025;3(1):56–73. doi:10.60141/ajid.68.
29. Centers for Disease Control and Prevention (CDC). Mpox: Data and research – case trends and demographics [Internet]. 2025 [cited 2025 Aug 12]. Available from: https://www.cdc.gov/mpox/data-research/cases/index.html
30. Idisi IO, Oshinubi K, Sewanu VB, Yahaya MM, Olagbami OS, Edogbanya HO. Investigating Mpox strain dynamics using computational and data-driven approaches. Viruses. 2025;17(2):154. doi:10.3390/v17020154.